PHOTONICS Research

Broadband athermal waveguides and resonators for datacom and telecom applications

Liuqing He,[1,2] Yuhao Guo,[1,2] Zhaohong Han,[3] Kazumi Wada,[3,4] Jurgen Michel,[3] Anuradha M. Agarwal,[3] Lionel C. Kimerling,[3] Guifang Li,[1,2,5] and Lin Zhang[1,2,*]

[1]Key Laboratory of Opto-electronic Information Technical Science of Ministry of Education, School of Precision Instruments and Opto-electronics Engineering, Tianjin University, Tianjin 300072, China
[2]Key Laboratory of Integrated Opto-electronic Technologies and Devices in Tianjin, School of Precision Instruments and Opto-electronics Engineering, Tianjin University, Tianjin 300072, China
[3]Department of Materials Science and Engineering, Massachusetts Institute of Technology, Cambridge, Massachusetts 02139, USA
[4]Department of Materials Engineering, University of Tokyo, Tokyo 113-8656, Japan
[5]College of Optics and Photonics, CREOL and FPCE, University of Central Florida, Orlando, Florida 32816, USA
*Corresponding author: lin_zhang@tju.edu.cn

Received 21 May 2018; revised 30 August 2018; accepted 31 August 2018; posted 5 September 2018 (Doc. ID 332312); published 8 October 2018

The high-temperature sensitivity of the silicon material index limits the applications of silicon-based micro-ring resonators in integrated photonics. To realize a low but broadband temperature-dependent-wavelength-shift microring resonator, designing a broadband athermal waveguide becomes a significant task. In this work, we propose a broadband athermal waveguide that shows a low effective thermo-optical coefficient of $\pm 1 \times 10^{-6}$/K from 1400 to 1700 nm. The proposed waveguide shows a low-loss performance and stable broadband athermal property when it is applied to ring resonators, and the bending loss of ring resonators with a radius of >30 μm is 0.02 dB/cm.

https://doi.org/10.1364/PRJ.6.000987

1. INTRODUCTION

Silicon photonics has been developed rapidly in the past ten years [1–4] because of seamless photonic integration with electronics and compatibility with mature CMOS fabrication technology. In silicon photonics, microresonator-based devices have the advantages of a small footprint, high performance, and low power consumption [5–7]. However, in contrast to electronic circuits that can function well with a temperature variation of tens of degrees celsius, integrated photonic devices, especially for microresonators, suffer from a high sensitivity to temperature, which has been an obstacle for their practical applications. This is due to the large thermo-optic coefficients (TOCs) of silicon used in integrated platforms. In an on-chip photonic system that may contain both active and passive devices, the local temperature of devices varies both spatially and temporally, which changes the refractive index and thus induces a large wavelength shift in resonator-based devices. At 1550 nm, the temperature-dependent wavelength shift (TDWS) of silicon is 110 pm/K [8]. For a high-Q microring resonator, this large wavelength drift may make the device completely unusable. Designing athermal photonic devices becomes an attractive solution to achieve temperature-insensitive integrated devices and systems.

To mitigate the thermal sensitivity of silicon photonic devices, some solutions have been proposed and demonstrated. An athermal technique is to utilize a Mach–Zehnder interferometer with asymmetric arms to fully compensate for the resonance shift [9], but this approach requires a large footprint and causes much power consumption. Besides, a heater or thermal feedback control [8,10,11] has also been used to stabilize the local temperature and the resonance wavelength, but it increases power consumption. Using negative thermo-optic polymer materials such as polymethyl methacrylate and hyperlinked fluoropolymer developed by Enablence [12] as cladding layers can compensate for the large positive TOC of Si. Polymer-cladded waveguides have been utilized to realize athermal filters [12–18] and modulators [19]. However, polymers show unstable properties with the change of environment conditions like thermal condition, mechanical strength, and moisture retention. A better candidate of negative-TOC materials is titanium dioxide (TiO_2), and it has a thermal expansion coefficient larger than the polarizability change due to thermal variations [20]. TiO_2 shows high stability during the fabrication process, and its negative TOC has been utilized to realize various athermal devices, including microresonators [21–23], modulators [24], arrayed waveguide gratings [25], filters [26], and lasers [27].

The effective TOC of an athermal waveguide, which consists of a Si core and a compensating material as cladding, can be expressed as Eq. (1). It is weighted by optical confinement

factors in different parts of the waveguide. By properly tailoring waveguide structural parameters, the negative-TOC material can fully compensate for the TDWS caused by positive-TOC material at a specific wavelength. However, as wavelength increases, the guided mode always extends to the negative-TOC cladding, and thus, the effective TOC of the waveguide becomes negative. This is why the previously reported athermal waveguides [13–27] can only achieve the athermal property at a single wavelength, which means that the zero TDWS can be produced for only one of the resonant peaks of a microresonator. However, for sensing and communication applications, it would be highly desirable to have wideband athermal devices:

$$\frac{\mathrm{d}n_{\mathrm{eff}}}{\mathrm{d}T}=\Gamma_c(\lambda)\frac{\mathrm{d}n_c}{\mathrm{d}T}+\Gamma_{cl}(\lambda)\frac{\mathrm{d}n_{cl}}{\mathrm{d}T}+\Gamma_{\mathrm{sub}}(\lambda)\frac{\mathrm{d}n_{\mathrm{sub}}}{\mathrm{d}T}. \quad (1)$$

In this work, we propose a broadband athermal waveguide, which shows a low effective TOC of $\pm 1\times 10^{-6}$/K from 1400 to 1700 nm. The proposed waveguide has a low-loss and bending-insensitive broadband athermal property when it is applied to ring resonators, and the bending loss of ring resonators with a radius of >30 μm is 1 dB/cm.

2. PRINCIPLE

A broadband athermal waveguide, as shown in Fig. 1, is based on a dual-cladding structure. The lower cladding, made by TiO_2, has a negative TOC, which compensates for the positive TOC of the Si core. By using another positive-TOC material, Si_3N_4, as an upper cladding, we can correct the wavelength dependence of the TOC to obtain a broadband athermal property. The key idea is to properly control the fractional powers of the guided mode in the core, the upper cladding, the lower cladding, and the substrate, $\Gamma_c(\lambda)$, $\Gamma_u(\lambda)$, $\Gamma_l(\lambda)$, and $\Gamma_{\mathrm{sub}}(\lambda)$, which are highly wavelength dependent, as expressed in Eq. (2). This requires a careful control of all the layer thicknesses. Thus, using TiO_2 instead of a polymer is advantageous in terms of both precise thickness and CMOS compatibility:

$$\frac{\mathrm{d}n_{\mathrm{eff}}}{\mathrm{d}T}=\Gamma_c(\lambda)\frac{\mathrm{d}n_c}{\mathrm{d}T}+\Gamma_u(\lambda)\frac{\mathrm{d}n_u}{\mathrm{d}T}+\Gamma_l(\lambda)\frac{\mathrm{d}n_l}{\mathrm{d}T}+\Gamma_{\mathrm{sub}}(\lambda)\frac{\mathrm{d}n_{\mathrm{sub}}}{\mathrm{d}T}. \quad (2)$$

Four structural parameters of this proposed waveguide can be tailored, which are waveguide width (W), Si_3N_4 cladding height (H_1), TiO_2 cladding height (H_2), and Si core height (H_3). The material TOCs of Si_3N_4, TiO_2, Si, and SiO_2 are 2.45×10^{-5}/K [28,29], -1×10^{-4}/K, 1.86×10^{-4}/K, and 1×10^{-5}/K [21], respectively. As wavelength increases, the optical confinement factors in both the TiO_2 cladding and the Si_3N_4 cladding become larger. At the beginning, the mode is mainly in the Si core and the TiO_2 cladding, and thus, the effective TOC decreases with wavelength. When the wavelength is long enough, the mode confinement factors in the Si_3N_4 layer and the SiO_2 substrate become significantly larger, and the effective TOC turns positive and increases with wavelength. In this way, one can infer from Eq. (2) that the effective TOC experiences a nonmonotonic change with wavelength, with two zero-TOC points.

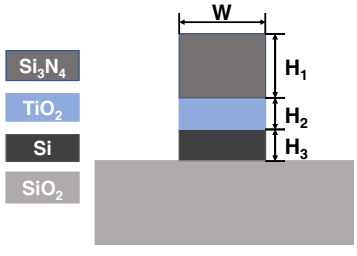

Fig. 1. Structure of the proposed broadband athermal waveguide, which consists of a Si core, a TiO_2 lower cladding, and a Si_3N_4 upper cladding.

Generally speaking, the TOCs of Si, Si_3N_4, and TiO_2 could vary with temperature and wavelength. For example, Si and Si_3N_4 are characterized in Refs. [30,31]. In practice, these should be measured, and the results would depend on a specific fabrication process in which the films are deposited. After being patterned to be optical waveguides, the stress in different layers may change, and designed parameters may have to be modified again to take the effect of stress into account [27].

3. RESULTS AND DISCUSSION

We calculate the effective TOC of the proposed athermal waveguide using a mode solver twice, with and without a temperature-induced index change added to the original material indices. Note that the material dispersion is taken into account for all the materials. The structural parameters W, H_1, H_2, and H_3 are 400, 250, 170, and 143 nm, respectively. The effective TOC is shown in Fig. 2. We note that the TOC curve of the proposed waveguide has two zero points, at 1450 and 1650 nm. By properly choosing the parameters above, the effective TOC remains within a small range of -1×10^{-6}/K in a wide wavelength band of 300 nm, from 1400 to 1700 nm. Mode fields of the athermal waveguide are shown in Fig. 2, which expand increasingly more into the lower cladding and then the upper cladding as wavelength increases. This confirms our idea above that a broadband athermal waveguide can be achieved by adding a positive-TOC material as the second cladding.

It is important to examine the impact of fabrication errors on the effective TOC. Specific to different fabrication steps, the error ranges are also different. We choose the error ranges of W, H_1, H_2, and H_3 to be ±10%, ±50%, ±5%, and ±1%,

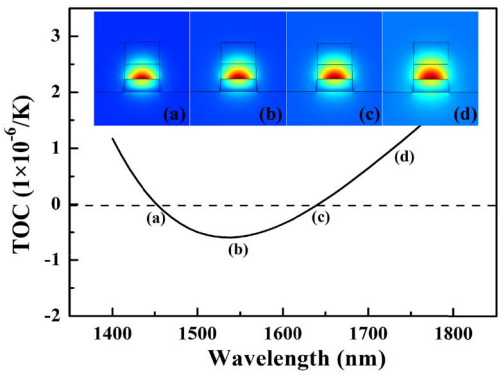

Fig. 2. Effective TOC of the proposed broadband athermal waveguide, with a small variation of $\pm 1\times 10^{-6}$/K in the waveband of 1400 to 1700 nm. The insets show the norm of the electric field, $|E|$, of the waveguide mode at different wavelengths, 1450, 1550, 1650, and 1750 nm, respectively.

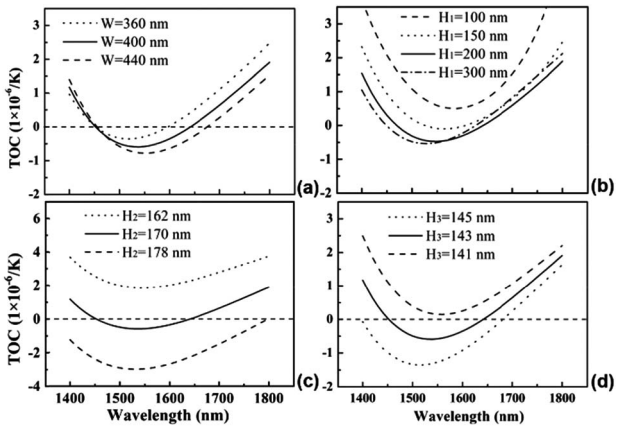

Fig. 3. Shifts of effective TOC curves when the structural parameters are changed, with (a) varied W of $\pm 10\%$, (b) varied H_1 of $\pm 50\%$, (c) varied H_2 of $\pm 5\%$, and (d) varied H_3 of $\pm 1\%$.

respectively. The Si core can have a precisely controlled thickness by oxidization, so we choose a small height variation for H_3, around $\pm 1\%$. The TOC changes caused by the fabrication errors are shown in Fig. 3. One can see that there is still a large bandwidth with athermal properties obtained with an effective TOC within $\pm 1 \times 10^{-6}$/K. We find that the effective TOC is quite insensitive to W and H_1 variations, especially for H_1. Width is typically less well-controlled in device fabrication, depending on lithography, and we see in Fig. 3(a) that the TOC curves are not changed much with a width variation of $\pm 10\%$. The Si_3N_4 layer is grown by chemical vapor deposition, and it can be controlled to be $\pm 5\%$, but here we intentionally increase the variation to show the robustness. Figure 3(b) shows that, as the positive-TOC material, Si_3N_4, has an increased height from 100 to 200 nm, the effective TOC curve counterintuitively becomes negative. This is because the Si_3N_4 layer will drag the optical field up, with more power into the negative-TOC material, TiO_2. As H_1 increases further to 300 nm, the TOC curve has a very limited shift because the fractional power of the mode in the SiO_2 substrate does not reduce due to an increased H_1, and thus, the mode profile is stabilized.

We note in Fig. 2 that the mode fields of the waveguide increasingly extend to the substrate as wavelength increases. With the same structural parameters, waveguide loss increases rapidly with wavelengths beyond 1860 nm, as shown in Fig. 4(a), but in the bandwidth of interest, with a small TOC, we have low loss due to substrate leakage. In simulations, we consider the Si_3N_4 film deposited using plasma enhanced chemical vapor deposition, in which N-H bonds may induce an absorption loss of 10 dB/cm. The propagation loss of the guided mode is found to be around 1 dB/cm over the wavelength range of interest. This is mainly due to the N-H absorption loss caused by Si_3N_4. This low-loss performance proves its compatibility with integrated photonic devices.

The proposed waveguide is the building block of a broadband athermal microresonator. When it is employed in microring resonators, the bending loss of the ring and the absorption loss of silicon nitride should also be taken into consideration. For comparison, we choose three bending radii, 100, 30, and 10 μm, and calculate the TOC and the optical loss of these

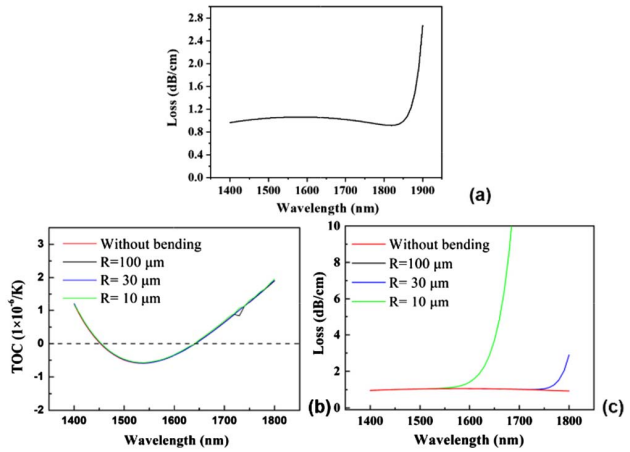

Fig. 4. (a) Optical loss of the proposed waveguide. It shows a low-loss performance in the bandwidth with a broadband athermal property. (b) Effective-TOC curves of the micro-ring resonators with different ring radii. (c) Bending loss with different radii. This shows a low-loss performance and a stable athermal property of the proposed broadband athermal micro-ring resonators.

micro-ring resonators. Figure 4(b) shows that the effective TOCs of the micro-ring resonators with different radii remain almost the same. This result shows the high insensitivity of the proposed broadband athermal resonators to the bending radius. In contrast, the optical loss of the micro-ring resonator increases greatly when the ring radius decreases. Nevertheless, the optical bending loss is still negligible for a ring radius of >30 μm over the wavelength range of interest from 1400 to 1700 nm. The relation between the TDWS and the effective TOC is given in Eq. (3) [12]. We calculate the TDWS of the broadband athermal ring resonator with a ring radius of 30 μm, as shown in Fig. 5. A variation within ± 0.5 pm/K in the wavelength range of 1400 to 1700 nm is obtained. Assuming the local temperature change is 30°C, this low TDWS is less than one resonance linewidth of a resonator with a cavity Q-factor smaller than 1×10^5:

$$\frac{1}{\lambda_r}\frac{\mathrm{d}\lambda_r}{\mathrm{d}T}(\lambda) = \frac{1}{n_g}\frac{\mathrm{d}n_{\mathrm{eff}}}{\mathrm{d}T}(\lambda). \tag{3}$$

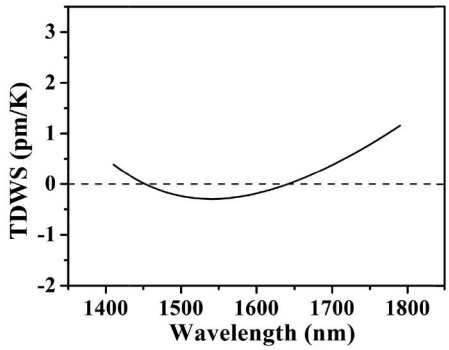

Fig. 5. TDWS of the microring resonator with a radius of 30 μm using the proposed waveguide. The TDWS is ± 0.5 pm/K in the wavelength range of 1400 to 1700 nm, corresponding to a wavelength shift of <15 pm with a temperature change of 30°C.

4. SUMMARY

We have proposed a broadband athermal waveguide and an associated ring resonator with low loss and a wideband and small TDWS of ±0.5 pm/K from 1400 to 1700 nm. This proposed resonator shows nearly unchanged temperature stability with different radii, which greatly broadens the applications of silicon ring resonators in multi-channel optical communications and broadband sensing systems.

Funding. National Basic Research Program of China (973) (2014CB340104/3); National Natural Science Foundation of China (NSFC) (61775164, 61335005, 61377076, 61575142, 61431009); Tianjin University.

REFERENCES

1. R. A. Soref, "The past, present and future of silicon photonics," IEEE J. Sel. Top. Quantum Electron. **12**, 1678–1687 (2006).
2. R. Kirchain and L. Kimerling, "A roadmap for nanophotonics," Nat. Photonics **1**, 303–305 (2007).
3. J. Leuthold, C. Koos, and W. Freude, "Nonlinear silicon photonics," Nat. Photonics **4**, 535–544 (2010).
4. R. Soref, "Mid-infrared photonics in silicon and germanium," Nat. Photonics **4**, 495–497 (2010).
5. B. E. Little, S. T. Chu, H. A. Haus, J. Foresi, and J.-P. Laine, "Microring resonator channel dropping filters," J. Lightwave Technol. **15**, 998–1005 (1997).
6. Q. Xu, D. Fattal, and R. G. Beausoleil, "Silicon microring resonators with 1.5-μm radius," Opt. Express **16**, 4309–4315 (2008).
7. I. Chremmos, O. Schwelb, and N. Uzunoglu, *Photonic Microresonator Research and Applications* (Springer, 2010).
8. K. Padmaraju, J. Chan, L. Chen, M. Lipson, and K. Bergman, "Thermal stabilization of a microring modulator using feedback control," Opt. Express **20**, 27999–28008 (2012).
9. B. Guha, B. B. C. Kyotoku, and M. Lipson, "CMOS-compatible athermal silicon microring resonators," Opt. Express **18**, 3487–3493 (2010).
10. G. Li, X. Zheng, J. Yao, H. Thacker, I. Shubin, Y. Luo, K. Raj, J. E. Cunningham, and A. V. Krishnamoorthy, "25 Gb/s 1V-driving CMOS ring modulator with integrated thermal tuning," Opt. Express **19**, 20435–20443 (2011).
11. B. Guha, K. Preston, and M. Lipson, "Athermal silicon microring electro-optic modulator," Opt. Lett. **37**, 2253–2255 (2012).
12. V. Raghunathan, W. N. Ye, J. Hu, T. Izuhara, J. Michel, and L. Kimerling, "Athermal operation of silicon waveguides: spectral, second order and footprint dependencies," Opt. Express **18**, 17631–17639 (2010).
13. Y. Kokubun, S. Yoneda, and S. Matsuura, "Temperature-independent optical filter at 1.55 mum wavelength using a silica-based athermal waveguide," Electron. Lett. **34**, 367–369 (1998).
14. J. M. Lee, D. J. Kim, H. Ahn, S. H. Park, and G. Kim, "Temperature dependence of silicon nanophotonic ring resonator with a polymeric overlayer," J. Lightwave Technol. **25**, 2236–2243 (2007).
15. W. Ye, J. Michel, and L. Kimerling, "Athermal high-index-contrast waveguide design," IEEE Photon. Technol. Lett. **20**, 885–887 (2008).
16. L. Zhou, K. Ken, K. Okamoto, R. P. Scott, N. K. Fontaine, D. Ding, V. Akella, and S. J. B. Yoo, "Towards athermal optically-interconnected computing system using slotted silicon microring resonators and RF-photonic comb generation," Appl. Phys. A **95**, 1101–1109 (2009).
17. P. Alipour, E. S. Hosseini, A. A. Eftekhar, B. Momeni, and A. Adibi, "Athermal performance in high-*Q* polymer-clad silicon microdisk resonators," Opt. Lett. **35**, 3462–3464 (2010).
18. J. Teng, P. Dumon, W. Bogaerts, H. Zhang, X. Jian, M. Zhao, G. Morthier, and R. Baets, "Athermal silicon-on-insulator ring resonators by overlaying a polymer cladding on narrowed waveguides," Opt. Express **17**, 14627–14633 (2009).
19. F. Qiu, A. M. Spring, H. Miura, D. Maeda, M. Ozawa, K. Odoi, and S. Yokoyama, "Athermal hybrid silicon/polymer ring resonator electro-optic modulator," ACS Photon. **3**, 780–783 (2016).
20. J. T. Bovington, "Athermal laser designs on Si and heterogeneous III-V/Si_3N_4 integration," Dissertations & Theses (Gradworks, 2014).
21. B. Guha, J. Cardenas, and M. Lipson, "Athermal silicon microring resonators with titanium oxide cladding," Opt. Express **21**, 26557–26563 (2013).
22. F. Qiu, A. M. Spring, F. Yu, and S. Yokoyama, "Complementary metal oxide semiconductor compatible athermal silicon nitride/titanium dioxide hybrid micro-ring resonators," Appl. Phys. Lett. **102**, 051106 (2013).
23. F. Qiu, A. M. Spring, and S. Yokoyama, "Athermal and high-*Q* hybrid TiO_2–Si_3N_4 ring resonator via an etching-free fabrication technique," ACS Photon. **2**, 405–409 (2015).
24. S. S. Djordjevic, K. Shang, B. Guan, S. T. S. Cheung, L. Liao, J. Basak, H.-F. Liu, and S. J. B. Yoo, "CMOS-compatible, athermal silicon ring modulators clad with titanium dioxide," Opt. Express **21**, 13958–13968 (2013).
25. H. Hirota, M. Itoh, M. Oguma, and Y. Hibino, "Athermal arrayed-waveguide grating multi/demultiplexers composed of TiO_2-SiO_2 waveguides on Si," IEEE Photon. Technol. Lett. **17**, 375–377 (2005).
26. T. Lipka, L. Moldenhauer, J. Müller, and H. K. Trieu, "Athermal and wavelength-trimmable photonic filters based on TiO_2-cladded amorphous-SOI," Opt. Express **23**, 20075–20088 (2015).
27. J. Bovington, S. Srinivasan, and J. E. Bowers, "Athermal laser design," Opt. Express **22**, 19357–19364 (2014).
28. A. Arbabi and L. L. Goddard, "Measurements of the refractive indices and thermo-optic coefficients of Si_3N_4 and SiO_x using microring resonances," Opt. Lett. **38**, 3878–3881 (2013).
29. I. E. Zadeh, A. W. Elshaari, K. D. Jöns, A. Fognini, D. Dalacu, P. J. Poole, M. E. Reimer, and V. Zwiller, "Thermo-optic characterization of silicon nitride resonators for cryogenic photonic circuits," IEEE Photon. J. **8**, 2701009 (2016).
30. G. Cocorullo, F. G. Della Corte, and I. Rendina, "Temperature dependence of the thermo-optic coefficient in crystalline silicon between room temperature and 550 K at the wavelength of 1523 nm," Appl. Phys. Lett. **74**, 3338–3340 (1999).
31. A. C. Hryciw, R. D. Kekatpure, S. Yerci, L. Dal Negro, and M. L. Brongersma, "Thermo-optic tuning of erbium-doped amorphous silicon nitride microdisk resonators," Appl. Phys. Lett. **98**, 041102 (2011).